Measurement of Impurity Emission Intensity Distribution in the Edge Region of LHD and Its Relation with Magnetic Field Structure*)

Taisuke KOBAYASHI[1)], Masahiro KOBAYASHI[1,2)], Arseniy KUZMIN[2)], Motoshi GOTO[1,2)], Hirohiko TANAKA[3)], Gakushi KAWAMURA[1,2)], Byron J. PETERSON[2)], Naofumi IWAMA[2)] and LHD Experiment Group[2)]

[1)]*SOKENDAI (The Graduate University for Advanced Studies), 322-6 Oroshi-cho, Toki 509-5292, Japan*
[2)]*National Institute for Fusion Science, 322-6 Oroshi-cho, Toki 509-5292, Japan*
[3)]*Graduate School of Engineering, Nagoya University, Furo-cho, Chikusa-ku, Nagoya 464-8603, Japan*

(Received 28 December 2017 / Accepted 16 March 2018)

In order to understand plasma transport in the edge stochastic layers, a visible spectrometer has been developed. Two-dimensional impurity emission intensity distributions in the edge stochastic layer of LHD, including divertor plate, divertor legs, X-point, and the last closed flux surface, have been measured. Carbon emission intensities and their distributions are found to be clearly different depending on the different magnetic field configuration and on the charge state. Effects of the edge magnetic field structure on these results are discussed.

Keywords: impurity emission, stochastic magnetic field, spectroscopy, divertor, two-dimensional measurement

DOI: 10.1585/pfr.13.3402030

1. Introduction

In magnetically confined fusion devices, control of impurity transport, such as exhaust of helium ash and screening of impurity coming from plasma facing components, is important for maintaining high performance plasma. In Large Helical Device (LHD), there is a stochastic magnetic field structure in the edge region due to the heliotron magnetic configuration [1]. Because of the very fast plasma transport parallel to the magnetic field lines compared to that perpendicular to the magnetic field, such magnetic field structure is considered to affect the transport of impurity as well as background plasma significantly [2]. The resulting impurity distribution then impacts on emission distributions, and thereby affects also detachment stability [3]. In LHD, the impurity emission measurements have been conducted, and correlation with the magnetic field structure and impurity transport are discussed [4]. However, the impurity transport property in the edge region is not yet fully understood. In order to address these issues, a visible spectrometer has been developed, which can measure impurity and hydrogen emission distributions in the edge region of LHD in detail. In this paper, we present recent measurement results conducted in the 19th experimental campaign of LHD. Effects of the edge magnetic field structure on the impurity emission distributions are discussed.

2. Experiment Setup

For two-dimensional (2D) emission distribution measurement in the edge region of LHD, a spectroscopy system has been developed. The spectrometer is equipped with a charge coupled device (CCD) camera as detector and with an array of 133 optical fibers. Figure 1 shows the field of view of the spectrometer and the fiber alignment. The red and yellow lines indicate divertor leg field lines, which connect to the different divertor plate arrays. Measurement region includes the divertor plates, diverter legs, X-point, and LCFS. The spectrometer can

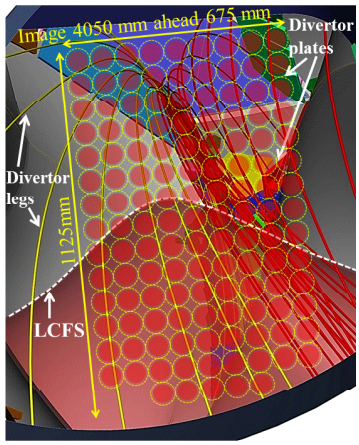

Fig. 1 Field of view and fiber alignment for the two-dimensional measurement. Yellow and red lines represent divertor legs, and dashed line indicates the LCFS.

author's e-mail: kobayashi.taisuke@lhd.nifs.ac.jp
*) This article is based on the presentation at the 26th International Toki Conference (ITC26).

change diffraction gratings remotely between 150, 300, and 2400 grooves/mm. In the present measurements, the grating of 150 grooves/mm is used for measurements of CII ($1s^2 2s2p3s\ ^4P^o$-$1s^2 2s2p3p\ ^4P$, 514 nm), and the grating of 2400 grooves/mm is used for CIII ($1s^2 2s3s\ ^3S$-$1s^2 2s3p\ ^3P^o$, 465 nm) and CIV ($1s^2 5f\ ^2F^o$-$1s^2 6g\ ^2G$, $1s^2 5g\ ^2G$-$1s^2 6h\ ^2H^o$, 466 nm).

The wavelength resolutions near the center of the CCD are 1.07 nm and 0.06 nm with the gratings of 150 and 2400 grooves/mm, respectively. Exposure time and cycle time are set to 0.09 - 0.19 sec and 0.2 - 0.3 sec, respectively, and were changed depending on the gratings and the plasma parameters.

In the present paper, the measurement results from two magnetic configurations (magnetic axis, R_{ax}) are presented: thin stochastic layer (R_{ax} = 3.60 m) and thick stochastic layer (R_{ax} = 3.90 m).

3. 2D Distribution of Impurity Emission

Figure 2 shows emission distributions of CII and CIV for the thin (R_{ax} = 3.60 m) and thick (3.90 m) stochastic layers with different densities. Figure 3 shows connection length (L_c) distributions on cross sections perpendicular to the line of sight (LOS) at a distance of 4.6 m (for thin stochastic case) and 4.0 m (for thick stochastic case) from the observation point. The different positions of the cross section for the two configurations are selected as representative positions for comparison of the emission distributions, as discussed below. The radial width of the stochastic layer, which is represented by yellow in Fig. 3, is clearly different between R_{ax} = 3.60 and 3.90 m. The configuration of R_{ax} = 3.90 m has a more complex structure at the periphery region. The dashed lines in Figs. 2 and 3 show characteristic magnetic field structures, such as divertor legs and LCFS.

Emission intensity distributions clearly change with the different magnetic field configurations. In the thick stochastic layer (Figs. 2 (c), (d)) case, the peak value is smaller and the emission region is distributed more widely in space as compared to the case of the thin stochastic layer (Figs. 2 (a), (b)). There is a secondary peak at the lower part of the figures (Figs. 2 (c-2) and (d-2)) in the thick stochastic case. This tendency becomes more evident in CIV in a high density discharge, as shown in Fig. 2 (d-2).

Since the emission distributions are integrated along the LOS, a direct comparison of the L_c distributions on a certain cross section is inappropriate. Nevertheless, taking into account the fact that the CII and CIV are mostly localized at the periphery of the plasma due to the low ionization potential (24 eV and 65 eV), we can discuss a possible relation with the magnetic field structure. It is found that the CII distribution in the thin stochastic layer case almost matches L_c distribution in the periphery region at 4.6 m from the observation point given in Fig. 3 (a). On the other hand, the CIV in the thick stochastic layer case matches the L_c distribution at 4.0 m (Fig. 3 (b)).

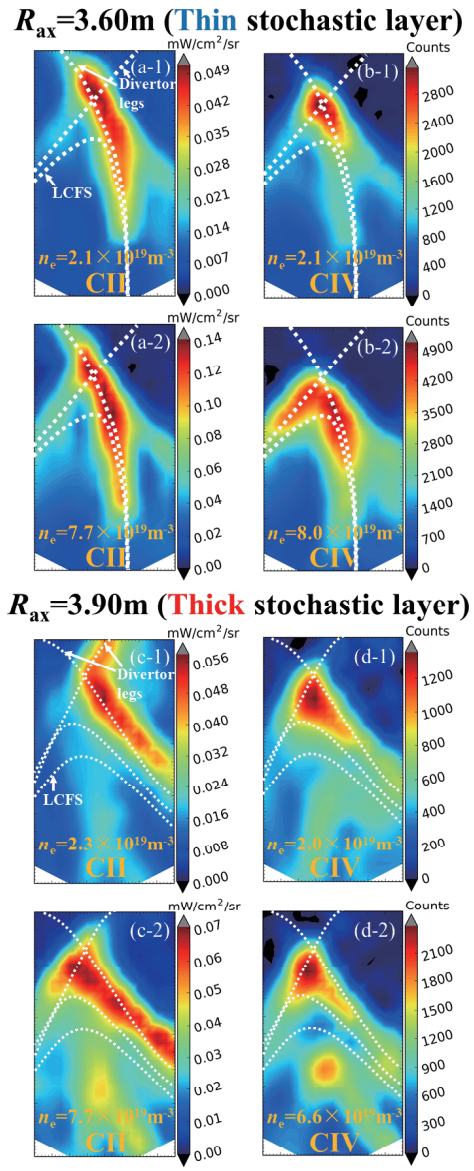

Fig. 2 2D Emission distributions of CII and CIV for (a), (b) thin stochastic layer (R_{ax} = 3.60 m) and (c), (d) thick stochastic layer (R_{ax} = 3.90 m). Left panels: CII. Right panels: CIV. Low (a-1, b-1, c-1, d-1) and high density (a-2, b-2, c-2, d-2) cases are shown.

3.1 CII emissions

As for the CII, the emission region extends toward the divertor plate along the left divertor legs (top left region in Figs. 2 (a-1) and (a-2)) in the thin stochastic layer case (3.60 m), while CII in the thick stochastic layer case (3.90 m) extends along right divertor legs (top right region in Figs. 2 (c-1) and (c-2)). This is considered to reflect plasma particle transport along divertor legs, which was found to change the dominant transport channel between the left and right legs in the different configurations [5]. With increasing the density, the CII distributions in the

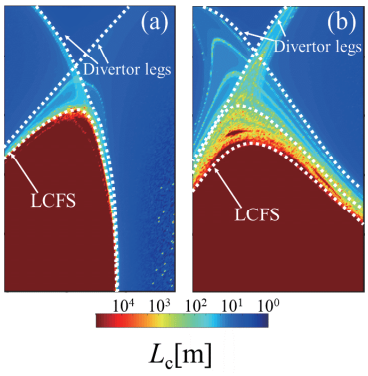

Fig. 3 L_c distributions at a plane perpendicular to the LOS with a distance of (a) 4.6 m from observation point in R_{ax} = 3.60 m. (b) 4.0 m in R_{ax} = 3.90 m.

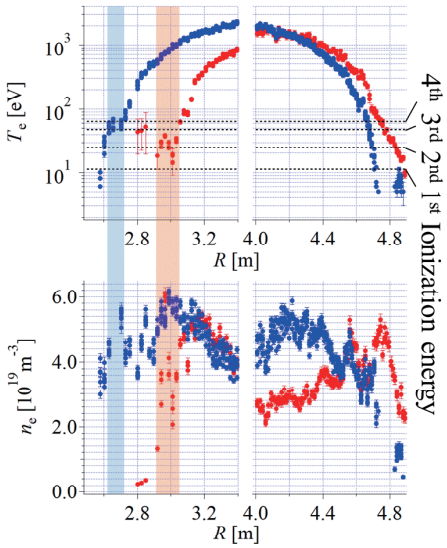

Fig. 4 T_e and ne profiles at $\overline{n_e}$ of 5×10^{19} m^{-3}. Blue and red symbols show cases of thin (R_{ax} = 3.60 m) and thick (R_{ax} = 3.90 m) stochastic layers. Black dashed lines indicate carbon ionization energy of different stages. The regions of T_e flattening are shaded with blue (R_{ax} = 3.60 m) and red (R_{ax} = 3.90 m).

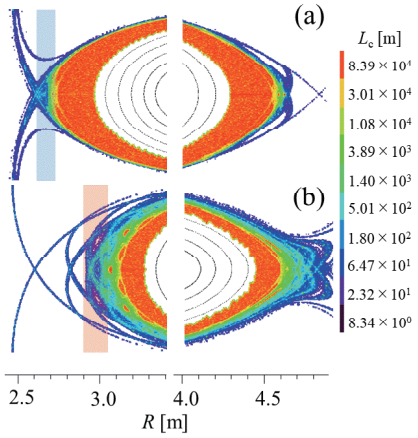

Fig. 5 L_c distribution. Red and blue shaded region correspond to T_e flattenings in Fig. 3. (a): B_t = −2.75 T, R_{ax} = 3.60 m, (b): B_t = −2.54 T, R_{ax} = 3.90 m

thick stochastic case change the patterns with the second peak appearing at the bottom center region (Fig. 2 (c-2)), while in the thin stochastic case the distribution remains in a similar pattern.

3.2 CIV emissions

As for the CIV, the emission is localized mainly around X-point and does not extend along the divertor legs. This is considered to be due to the different ionization potentials between the two charge states. That is, CIV is emitted in region closer to LCFS than CII emissions. Slight broadening of CIV emission around X-point is observed in thin stochastic (Fig. 2 (b-2)). This is considered to be due to the electron temperature (T_e) profile in the edge region.

Figure 4 shows electron temperature (T_e) and density (n_e) profiles at the edge region along the midplane obtained by the Thomson scattering system with the line averaged density of 5×10^{19} m^{-3}. All data points during the exposure time of the emission measurements are plotted. It is found that there is a clear flat T_e region at the inboard side, 2.63 < R < 2.74 m (shadowed with blue), in the thin stochastic layer, which corresponds to the ionization potential between the 3rd and the 4th charge states. In the case of the thick stochastic layer, the flattening occurs at 2.92 < R < 3.03 m (shadowed with red), which corresponds to the potential between the 2nd and the 3rd ionization energy. In these temperature ranges C^{3+} ions (CIV) and C^{2+} ions (CIII), respectively may dominantly exist due to its ionization potential. On the outboard side, on the other hand, there appears no clear T_e fattening. This is considered due to the spatial phase of remnant island chains in the stochastic layer relative to the midplane (measurement line of Thomson system), as discussed in ref. [6].

Shown in Fig. 5 are the connection length distributions in the edge region of LHD for R_{ax} = 3.60 and 3.90 m to be compared with the T_e and n_e profiles. Thickness of stochastic field layer for R_{ax} = 3.90 m is larger than for R_{ax} = 3.60 m. It is seen that the T_e flattening of the thin stochastic layer corresponds to the X-point region of the divertor legs, while that of the thick layer corresponds to the stochastic region as indicated by the shaded area in the figure. The results clearly show that the T_e profiles are strongly affected by the edge magnetic field structure. Plotted in Fig. 6 is T_e profiles around the flattening region in the thin stochastic case for densities of n_e = 2.1, 5.7 and 7.6 × 10^{19} m^{-3}, respectively. The T_e in the flattening region is higher than 4th ionization potential for n_e = 2.1 × 10^{19} m^{-3}, which corresponds to the density of Fig. 2 (b-1). On the other hand, T_e gradually decreases and becomes below the 4th ionization potentials for 5.7 × 10^{19} m^{-3}, which can lead to enhancement of CIV emission, as observed in the spatial broadening in Fig. 2 (b-2).

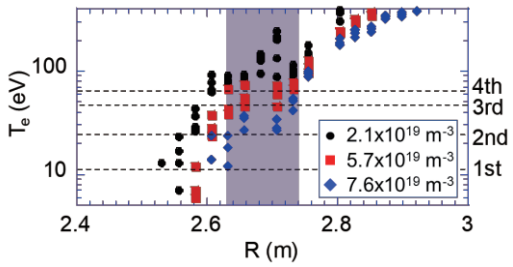

Fig. 6 Radial profiles of T_e around flattening region in R_{ax} = 3.60 m (thin stochastic case) for n_e = 2.1, 5.7, and 7.6 × 10^{19} m^{-3}.

From these results, it is clearly shown that impurity emission intensity distribution largely depends on its charge state, and is strongly affected by a difference in the magnetic field structure. A tomography analysis, which is currently under development, will spatially resolve the emission intensity distribution along the LOS, and its relation with the magnetic field configuration will be studied in more detail in future.

4. Density Dependence of Impurity Emission

4.1 CII emissions

Figure 7 shows density dependences of impurity emission intensity for different charge states and different magnetic configurations (thin and thick stochastic layer), where the intensity is averaged over the field of view. Density dependences are clearly different between charge states and between magnetic configurations. In the case of thin stochastic layer (R_{ax} = 3.60 m), CII emission increases with electron density up to $n_e \cong 6 \times 10^{19}$ m^{-3}, and then it starts to roll-over. In the case of thick stochastic layer (R_{ax} = 3.90 m), CII emission saturates at lower density, $n_e \cong 3 \times 10^{19}$ m^{-3}, and then starts to decrease. It is considered that CII emission reflects carbon source amount generated by sputtering of divertor plates. The divertor particle flux in toroidal section 7, which is close to the measurement area, is plotted as a function of density in Fig. 8, where "R" and "L" denote right and left divertor arrays, respectively. The CII intensity in thin stochastic case behaves in a way similar to the particle flux at 7L, which saturates at $n_e \cong 6 \times 10^{19}$ m^{-3} and then slightly decreases. In the case of thick stochastic layer, the early saturation at $n_e \cong 3 \times 10^{19}$ m^{-3} is also seen in the divertor flux. In the higher density range, however, the divertor particle flux starts to increase again while the CII intensity continues to decrease. It may be due to change of sputtering coefficient in the high density range.

4.2 CIII and CIV emissions

CIII emissions are almost the same between the two configurations. On the other hand, CIV emission in the case of the thick stochastic layer is about one-half of those

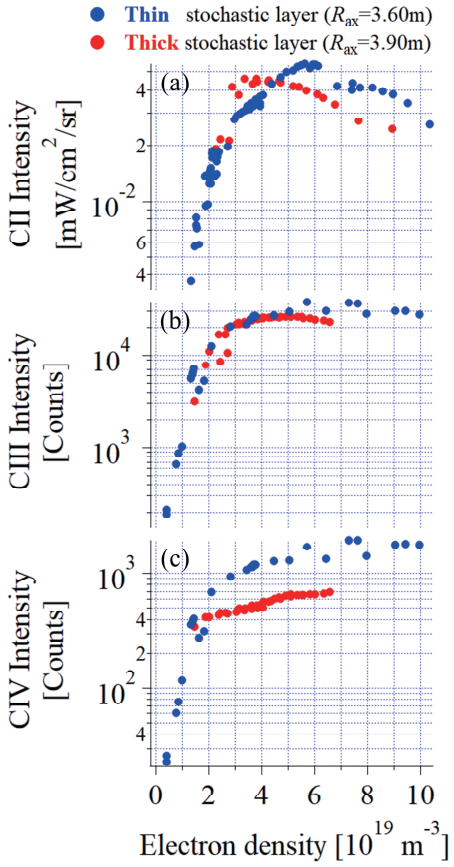

Fig. 7 Density dependences of average emission intensity of (a) CII, (b) CIII, and (c) CIV. Blue and red symbols show cases of thin (R_{ax} = 3.60 m) and thick (R_{ax} = 3.90 m) stochastic layer.

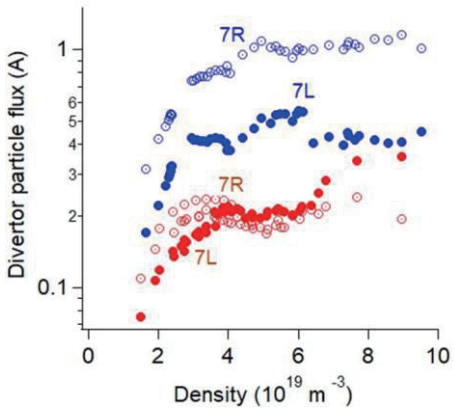

Fig. 8 Divertor particle flux obtained by Langmuir probe at toroidal section 7. Blue: R_{ax} = 3.60 m (thin stochastic case). Red: R_{ax} = 3.90 m (thick stochastic case). "R" and "L" denote right and left divertor arrays.

of the thin stochastic layer. This difference is larger than those observed in CII emission, that is, the difference in the carbon source amount. As a possible interpretation of the noticeable difference in CIV, effect of edge plasma parameters is discussed as follows.

Assuming ionizing plasma, emission intensity for charge state Z measured in the experiments can be written as

$$l_Z(p,q) = R_1(p) n_e n_Z(1) V A(p,q). \quad (1)$$

Here, p and q are energy level ($p > q$). $n_Z(p)$, V, $A(p,q)$, $R_1(p)$ and n_e are population density of level p, volume of emission region, spontaneous transition probability, population coefficient, and electron density, respectively. $p = 1$ means ground state. The observed emission intensities are proportional to electron density, density of carbon of charge state Z, and volume where carbon exists,

$$l_Z(p,q) \propto n_e n_Z(1) V. \quad (2)$$

In the case of thin stochastic layer ($R_{ax} = 3.60$ m), the volume for CIV emission is considered to become large due to the T_e flattening at the inboard side (Figs. 4 and 6), i.e., $n_Z(1)V$ is larger. At the same time n_e is the same or larger than the thick layer case ($R_{ax} = 3.90$ m) at the very edge region. This can lead to larger emission intensity of CIV in the thin stochastic case (3.60 m) according to eq. (2), which is consistent with the observation in Fig. 7 (c).

On the other hand, T_e flattening (red region in Fig. 4) in the thick layer case ($R_{ax} = 3.90$ m) can widen the CIII emission volume due to the ionization potential of CIII. However, CIII intensity in 3.90 m is not larger than 3.60 m. This is considered due to the lower n_e in the flattening region in the thick case, which already dropped to ~ 2 to 4×10^{19} m^{-3}.

More consistent argument should be made taking into account transport effects and the magnetic geometry effects. Such research is currently in preparation. Nevertheless, from the above results, it is suggested that magnetic field structure in the edge region influences impurity emission intensity and its distribution significantly.

5. Summary

In order to study impurity emission distribution and its relation to the edge magnetic field structure, carbon emission intensities and the 2D distributions have been measured. It is revealed that density dependence of impurity emission intensities is different for different charge states and different magnetic field configurations. The results are interpreted as due to the change of background plasma temperature and density profiles caused by magnetic configuration. It is also found that the 2D impurity emission distributions change significantly depending on the charge states and magnetic field configurations. These results suggest the important role of magnetic field structure on the impurity emission and transport.

Acknowledgments

The authors are grateful to Dr. T. Nakano for the fruitful discussions. This work has been financially supported by JSPS Grant No. 16H04622, and by the NIFS budget ULPP026 and GGPP001.

[1] N. Ohyabu *et al.*, Nucl. Fusion **34**, 387 (1994).
[2] M. Kobayashi *et al.*, Nucl. Fusion **55**, 104021 (2015).
[3] M. Kobayashi *et al.*, Nucl. Fusion **53**, 093032 (2013).
[4] H. Zhang, S. Morita *et al.*, Phys. Plasmas **24**, 022510 (2017).
[5] M. Shoji *et al.*, J. Nucl. Mater. **390-391**, 490 (2009).
[6] Y. Feng *et al.*, Nucl. Fusion **48**, 024012 (2008).